The Role of Sea Surface Temperatures in Interactions Between ENSO and the North Pacific Oscillation

David W. Pierce

Climate Research Division, Scripps Institution of Oceanography

La Jolla, California

Submitted to Journal of Climate

December 8, 2001

Abstract

The North Pacific Oscillation (NPO) is a decadal to interdecadal fluctuation of sea surface temperatures (SSTs) in the North Pacific. Previous workers have shown that during individual El Nino and La Nina winters, atmospheric circulation anomalies over North America are characteristically different for different phases of the NPO. Two physical mechanisms could account for this observed link between North Pacific SSTs and ENSO's effects over North America. 1) NPO SSTs could force changes in the overlying atmosphere that modulate ENSO's effects. 2) The atmosphere could undergo internal variability that both modulates ENSO's effects and imprints a characteristic pattern of North Pacific SSTs. The first mechanism suggests methods for increasing the skill of seasonal climate predictions by incorporating the state of the North Pacific, using simple persistence of SSTs if nothing else. The second mechanism implies that North Pacific SSTs add no information that could be used to improve seasonal climate predictions of ENSO's effects. Analysis of a 300-year run of a coupled ocean-atmosphere model shows that it exhibits links between NPO and ENSO similar to those observed. It is found that specifying NPO SSTs does *not* force these links. This suggests that the association found between NPO SSTs and ENSO's effects is primarily because both are responding to the same internal atmospheric variability. In such a case, incorporating accurate predictions of NPO SSTs into ENSO prediction schemes would have little ability to improve forecasts of ENSO's effects.

1. Introduction

The El Niño-Southern Oscillation (ENSO) phenomenon has important global effects on climate, including winter conditions over North America (e.g., Wallace and Gutzler (1981); Lau (1985); Ropelewski and Halpert (1986)). Efforts to improve seasonal forecasts of ENSO's effects could therefore have useful societal payoffs in addition to being a scientifically interesting problem.

Gershunov and Barnett (1998; GB hereafter) found that ENSO's effects over North America are strongly associated with the state of the North Pacific Oscillation (NPO), as determined from the NPO's characteristic signature in sea surface temperatures (SSTs). Following GB, this will be referred to as the "modulation" effect. As an example, sea level pressure (SLP) over the northeastern Pacific during an El Niño is strongly negative when the NPO is in its high state, but neutral or weakly positive during NPO's low state. The existence of this relationship between North Pacific SSTs and ENSO's effects raises the possibility that including information from North Pacific SSTs could improve the seasonal forecast skill of climate models, at least during El Niño or La Niña years. The purpose of this study is to test this possibility in the context of a coupled global ocean-atmosphere model.

Two mechanisms could account for the link between NPO SSTs and ENSO's effects as found by GB: 1) *SST forces*: low-frequency changes in North Pacific SSTs force changes in the overlying atmosphere that modulate ENSO's effects over North America. 2) *SST responds*: the atmosphere undergoes internal variability that both modulates ENSO's effects and characteristically imprints North Pacific SSTs. Of these two mechanisms, the first

(SST forces) might be useful for predictions, as North Pacific SSTs may be predictable on a seasonal timescale (by persistence or wintertime reemergence of subducted anomalies if nothing else). The second mechanism (SST responds) is not useful for predictions of ENSO's effects over North America, if it is the only thing happening (ignored here is any information gained by considering the North Pacific ocean an *in-situ* atmospheric observing system). This is true even if the SSTs themselves are predictable by persistence or other mechanisms, as (by hypothesis if SST *only* responds) the atmosphere is unaffected by the midlatitude SST anomalies in this case. Of course, the real world might have these two mechanisms operating simultaneously in the form of a coupled ocean-atmosphere mode, with SST both responding to and forcing the atmosphere (e.g., Latif and Barnett 1994, Pierce et al. 2001).

The purpose of this study is to determine how much of the NPO-ENSO link found by GB arises from the *SST forces* versus the *SST responds* mechanism. This question is examined by using the parallel climate model (PCM; Washington et al. 2000), which is briefly described in Section 2. In Section 3 a 300-year control run of PCM is analyzed, and shown to exhibit a link between NPO and ENSO similar to, although weaker than, found in the observations. In Section 4a the Pacific-wide SST fields associated with the following four cases are extracted from the control run: El Niño-High NPO, El Niño-Low NPO, La Niña-High NPO, and La Niña-Low NPO. These SST fields are used to force the atmospheric component of PCM (Section 4b), where it is shown that the link between NPO and ENSO is *not* reproduced by specifying SSTs. Since the model has the NPO-ENSO link in the first place, this indicates that the predominate mechanism is *SST responds*. The

results are discussed in Section 5 and conclusions given in Section 6.

2. The Parallel Climate Model

The parallel climate model (PCM) is a state of the art, fully coupled ocean-atmosphere general circulation model (Washington et al. (2000); see also http://www.cgd.ucar.edu/pcm). The atmospheric component of the PCM is the CCM3 atmospheric general circulation model (Kiehl et al. 1998), used here at T42 resolution (equivalent to about 280 by 280 km grid spacing). CCM3 includes a land surface model that accounts for soil moisture and vegetation types. The ocean component of PCM is the Parallel Ocean Program (POP; Smith et al. 1992, Dukowicz and Smith 1994), used here at a horizontal resolution of 384 by 288, with 32 vertical levels. A displaced-pole grid is used in the northern hemisphere to eliminate the problem of convergence of the meridians in the Arctic Ocean. A dynamic-thermodynamic sea-ice model based on Zhang and Hibler (1997) is included, with an elastic-viscous-plastic rheology for computational efficiency (Hunke and Dukowicz 1997).

Although a complete description of PCM's base state and variability is outside the scope of this article, Fig. 1 shows the leading empirical orthogonal functions (EOFs) for the ENSO and NPO modes of SST variability, which are directly relevant to our purpose here. The corresponding observed patterns computed from observations (da Silva et al. 1995) are also shown for comparison.

The ENSO mode shown is the leading EOF of Pacific-wide annually averaged SST anomalies, and accounts for 29% of the variance in the model and 33% of the variance in the observations. The equatorial SST signal associated with one standard deviation (1σ) of the

associated principal component (PC) is 0.8°C in the model and 0.6°C in the observations. The model's equatorial cold tongue variability extends too far to the west, a common failing of coupled ocean-atmosphere general circulation models (Mechoso et al. 1995). Also, the southern hemisphere expression in SST is weak compared to the observations. The work here will be confined to the northern hemisphere.

The NPO mode is the leading EOF of detrended SSTs north of 20° N averaged over December, January, and February (DJF). It accounts for 26% of the variance in the observations and 35% of the variance in the model. The central North Pacific SST signal associated with 1σ of the PC is 1.1°C in the model and 0.7°C in the observations. The geographical pattern of the model's NPO is similar to the observed, although with too much positive loading along the west coast of North America. Following GB, the NPO will be termed "high" in the phase illustrated in Fig. 1, with colder than usual conditions in the central North Pacific and warm anomalies along the west coast of North America, and "low" during the reversal of this pattern.

3. Association Between NPO and ENSO in the Control Run

The observed dependence of SLP anomaly on the state of ENSO and the NPO, as found by GB, is shown in their Fig. 2. Their data are replotted here in Fig. 2 for convenience. Focusing first on the El Niño response (left column of Fig. 2), the SLP anomaly in the Aleutian low region is, on average, -4.5 mb. When the NPO is high, the SLP anomaly is -8 mb; when the NPO is low, the anomaly is only weakly negative or slightly positive. Over the Atlantic, the amplitudes are similar between the high and low NPO cases, about -3 mb, but the significant response shifts to the east when the NPO is low. Overall, the

pattern is more wave-like in the high NPO case, with centers of action over the Aleutian region, Hudson Bay, and southwest Atlantic, while it is more NAO-like when the NPO is low.

During La Niña (right column of Fig. 2), the SLP anomaly in the Aleutian region is 5 mb when the NPO is low, but only 1 mb when the NPO is high. The response in the Atlantic is 1.5 mb when the NPO is low, but 4.5 mb when it is high. There is also a strong response over the central U.S., which typically experiences moderately low SLP when the NPO is low but distinctly high SLP anomalies when the NPO is high.

For a given ENSO state (either El Niño or La Niña), the difference in SLP anomalies between high and low phases of the NPO gives an estimate of the NPO's contribution to the anomalies when linearity is assumed. This is shown in Fig. 3; Fig. 3a is Fig. 2c minus Fig. 2e, and Fig. 3b is Fig. 2d minus Fig. 2f. Significance of these difference fields is not computable using only the data from Fig. 2, and so no significance levels are indicated. In the absence of sampling errors, and if the NPO and ENSO were independent and interacted only linearly, then there would be no difference between panels a and b of Fig. 3. The degree to which the differences actually seen are due to sampling errors is discussed in Section 5.

To check whether these observed changes in SLP were reproduced in the numerical model, the PCM's 300-year "B04.10" control run was analyzed in a manner similar to that used for the observations in GB. One of GB's key points was to consider a time scale separation between ENSO and the NPO, with ENSO periods in the 2-7 yr band and NPO periods longer than 10 years. The purpose of this was to see if the state of a slowly chang-

ing, persistent phenomenon (the NPO) could be used to predict the teleconnected effects of the faster changing ENSO. To enforce this scale separation, the ENSO index used here was determined by forming an index based on DJF SSTs in the nino3.4 region (180 to 140°W, 5°S to 5°N), filtered to include only periods shorter than 10 years cycle^{-1}. (Results of sensitivity tests using unfiltered versions of the ENSO and NPO indices are discussed in Section 5.) A year was considered to be an "El Niño" or "La Niña" only if the nino3.4 index was more than 0.8σ away from zero. Following GB, the main field analyzed will be SLP averaged over January, February, and March (JFM). The one-month lag compared to the DJF SST index is done to match GB, who used this offset because the ENSO response is more stationary during JFM than DJF.

GB do not form a NPO index *per se*, but use time periods associated with interdecadal regime shifts identified by Mantua et al. (1997). As noted above, the motivation for doing this was to composite based upon the low-frequency, persistent part of the NPO. To emulate this, the NPO index used here was PC of the leading EOF of 10-year low pass filtered North Pacific SSTs. A year was considered "high" or "low" NPO depending on the sign of this index. Using these criteria, the model yields 27, 25, 27, and 34 winters for the El Niño-high NPO, El Niño-low NPO, La Niña-high NPO, and La Niña-low NPO cases, respectively. With 60 years of observed data, GB found 8, 7, 5, and 7 winters.

The results for SLP anomaly are shown in Fig. 4. Shading indicates where the response is different from the control run at the 95% significance level. The ENSO response averaged over all NPO states (upper two panels) is similar to the PNA pattern (Horel and Wallace 1981), with negative values in the Aleutian low region, positive values over Hudson Bay,

and negative values over the Southeastern U.S. during El Niño, and a similar pattern with reversed sign during La Niña. Note that the model is more linear than the observations, in the sense the La Niña response looks similar to a negated El Niño response. The response also extends too far eastwards, which suggests that results over the Atlantic sector may be less robust than those over the Pacific or North America.

Consider first the El Niño response (left hand column of Fig. 4). When the NPO is high, the SLP anomaly in the Aleutian low region deepens from -5 mb (panel a) to -7 mb (panel c). The observations show a deepening from -4.5 to -8 mb. Over the Atlantic, the model is nearly unchanged at -2 mb, while the observations show a slight weakening from -2 to -1 mb.

When the NPO is low (Fig. 4, panel e), the SLP response shifts southeastwards and weakens to -2 mb in the Aleutian low region (shifts southeast and weakens to -1.5 mb in the observations). Over the Atlantic, the response is nearly unchanged but loses statistical significance (no weakening in the observations, but statistical significance is also lost). Overall, the model's response for El Niño conditions is quantitatively similar to the observations.

For La Niña conditions (right hand column of Fig. 4), the SLP response in the Aleutian low region strengthens from 6 mb (panel b) to 7 mb (panel f) when the NPO is low, and weakens to 5 mb (panel d) when the NPO is high. The corresponding observed values are a strengthening from 3.5 to 4.5 mb, and a weakening to 1 mb, respectively. Over the Atlantic, the SLP increases slightly, going from about 1.5 to 2 mb when the NPO is high (observations show an increase from 2.5 to 4.5 mb), and slightly weaken and lose

some statistical significance when the NPO is low (observations show both the loss of significance and a weakening to 1.5 mb). Overall, the model's response in the La Niña case is in the same direction as seen in the observations, but the patterns are noticeably more different from the observed than seen in the El Niño case. In particular, the observations indicate a 2mb reversal of SLP over the central U.S. when going from high to low NPO that the model misses entirely.

The difference between the SLP anomalies in the high and low NPO states, for a given ENSO state (either El Niño or La Niña), is shown in Fig. 5. For both ENSO states, the primary effect of the NPO on ENSO's response lies in the North Pacific, where the NPO itself has its peak response. In addition, during El Niño there is a small region of significant response over the southeast U.S., while during La Niña there is a similar feature over the eastern Atlantic. These difference fields can be directly compared to Fig. 3, which illustrates the same quantity for the observations. In both the model and observations, the El Niño case shows maximum response over the Aleutian Low region at about 160 W, 50 N, while the response is shifted north and compressed in the north-south direction in the La Niña case. In the La Niña case, the ridge of positive anomalies that can be seen stretching from the central U.S. to the Pacific Northwest is not reproduced by the model. This is discussed more in Section 5 (Fig. 13).

In summary, the model shows systematic differences in ENSO's wintertime SLP response depending on whether the NPO is in the high or low state. The largest signal and best agreement between model and observations is over the Aleutian low region. The model's El Niño response is more like the observations than the La Niña response; while

the El Niño and La Niña responses in the model are approximately anti-symmetric, this is less true in the observations.

GB do a further analysis in terms of heavy precipitation frequency (HPF), making use of daily rainfall totals. Only monthly data were saved in the pre-existing control run used here, so the same analysis cannot be performed. Instead, monthly averaged precipitation totals have been used, again averaged over JFM. The results from the control run are shown in Fig. 6. Illustrated are the composite anomalies for the four ENSO/NPO cases, along with the difference (high minus low NPO) for the two ENSO states. During El Niño(panels a and c), the west coast and southeast part of the U.S. both have greater than normal precipitation. The positive anomaly over the far eastern Pacific is larger during the low phase of the NPO than during the high phase (although the difference is barely significant – panel e). During La Niña (panels b and d), the west coast and southeast U.S. are drier than normal. Given the limited areas of significance seen in panels e and f, most of the differences between the high and low NPO response can be explained by sampling variability.

4. Forced Experiments

The purpose of the forced experiments is to see whether the systematic difference in ENSO SLP and precipitation response between the high and low NPO cases is determined by SSTs (*SST forces*) or insensitive to SSTs (*SST responds*). To that end, the SST patterns associated with the four cases (El Niño-high NPO, El Niño-low NPO, La Niña-high NPO, and La Niña-low NPO) will be computed and applied as lower boundary conditions to the same atmospheric model used in the control run. The results will then be compared to the control run results described above.

a. Composite SST fields

The SST fields corresponding to the various ENSO/NPO cases are shown in Fig. 7. These were obtained by compositing on the indices described above. Two points regarding the SST fields are worth noting.

First, by taking composites, we include the possibility that systematic changes in tropical Pacific SSTs between high and low NPO conditions account for the modulation effect. One hypothesis for the modulation effect might be that systematic differences in tropical SSTs both force the NPO and result in different expressions of extratropical SLP response, thereby completely accounting for the modulation effect. By keeping these systematic differences in tropical SSTs in the forcing fields, this hypothesis will be tested in the experiments. (In practice, Fig. 7 shows that these differences are small, and it will later be concluded that this hypothesis does not explain the modulation effect.)

Second, the SST fields in Fig. 7 might, at first glance, look rather different than expected. In particular, they do *not* look like plus and minus the tropical part of the ENSO signal (Fig. 1, panel b) glued together in the extratropics with plus and minus the NPO signal (Fig. 1, panel d). Note, for example, how the North Pacific SSTs in Fig. 7, panels d and e bear only passing resemblance to the single lobe of anomalies extending out from Japan, surrounded by a horseshoe of opposite sign, that can be seen in Fig. 1. Instead, as shown in Fig. 8, the composites look much more like the basin-wide, point-by-point sum of the ENSO (Fig. 7 a, b) and NPO SST anomalies (Fig. 8 a, b). This should be kept in mind when designing specified-SST experiments to examine the NPO.

b. Results of forced experiments

The SST anomaly fields shown in Fig. 7 were added to PCM's monthly SST climatology, and imposed as the lower boundary condition to the PCM's atmospheric model, CCM3. For each of the four cases (El Niño/La Niña combined with High-NPO/Low-NPO), the model was run for 25 years, and the SLP fields analyzed as above. Anomalies were obtained by subtracting out the 300-year control run's climatology. Note that these are not "constant January" type experiments; the forcing and surface conditions change continually, but the SST *anomalies* are held fixed.

The results are shown in Fig. 9. Considering the El Niño results first (left hand column), in the Aleutian region the difference between the high and low NPO cases is less than 1 mb (compared to a difference of 4-5 mb in the control run). There is little ($<$1 mb) difference found over the central-southeastern U.S. Over the Atlantic, there is an appreciable difference found, with pressures 4 mb lower during the high NPO state than during the low NPO state. Note that this feature was not present in the control run.

For the La Niña case (right hand column of Fig. 9), in the Aleutian low region, there is virtually no difference between the high and low NPO cases, compared to a difference of about 3 mb in the control run. Again, there is a difference over the Atlantic (of about 2 mb), where no difference was found in the control run.

The previous figures show where the forced run's responses are significantly different from the control run. However, the main purpose here is to find where the response during high NPO conditions is different from that during low NPO conditions. To that end, use will be made of three regions of interest: the Aleutian region (180 to 150°W, 40°N to 65 °N), the southeastern U.S. (90°W to 70°W, 20°N to 30°N) and the Atlantic (40°W to

10°W, 40°N to 55°N). The sequence of SLP anomalies for each case averaged over the region of interest was determined, then normalized by the control run's standard deviation in the region (cf. Hegerl et al. (1996) for optimal detection methodologies). A two-sided Kolmogorov-Smirnov (K-S) test (Press et al. 1992) was used to determine the likelihood that the SLP sequences for the high and low NPO cases were actually drawn from the same underlying distribution, differing only due to expected sampling variations. Likelihoods less than 0.05 will be considered significant.

The histogrammed sequences for the El Niño case during JFM are shown in Fig. 10. The control run shows significant differences in SLP between the high and low NPO cases over the southeast U.S. and Aleutian region, but none in the Atlantic. The forced run shows no significant differences between the high and low NPO cases in any region, although it should be noted that the difference in the Atlantic sector would be significant at the 90% confidence level.

The results for the La Niña case are shown in Fig. 11. Significant differences are found in the Aleutian region in the control run, but no significant differences between high and low NPO are found in the forced run in any region.

In summary, the SLP response to high versus low NPO SST conditions in the forced case failed to consistently reproduce the SLP response found in the control case.

The results of the forced experiments in monthly averaged precipitation are shown in Fig. 12. Comparing to the precipitation results for the control run (Fig. 6), it can be seen that the forced runs capture virtually none of the control model's association between ENSO and NPO. The only exception might be the positive values over the gulf of Alaska seen

in the difference between NPO states (high minus low) during La Niña. Balanced against this is that the control run had a very similar response during El Niño, while the forced experiments do not. In general, the control run's only consistent effect of the NPO on monthly averaged precipitation was along the west coast of North America; the forced experiments fail to reproduce this. Comparing the control and forced responses over the Atlantic shows that the forced model does not reproduce the control run in that region either.

5. Discussion

The results outlined above support the idea that the observed link between the NPO and ENSO arises primarily because the atmosphere undergoes internal variability that both modulates ENSO's effects and characteristically imprints North Pacific SSTs. Deser and Blackmon (1995) suggested that the mechanism for this imprinting might be changes in latent heat flux associated with alterations in surface wind. This was found to be the case in a numerical model, at least for year-to-year variability, by Pierce et al. (2001); Ekman transport, and cloud changes that alter the solar heat flux, were found to be important as well. At the longer (multiyear to decadal) time scales traditionally associated with the NPO, Schneider et al. (2001) find that Ekman transport and vertical mixing processes become dominant.

Another hypothesis that might explain the modulation effect is that systematic changes in tropical SSTs between different ENSO events both force the NPO and result in different midlatitude expressions in SLP. If this were the entire basis for the modulation effect, then the forced experiments (which included all differences in tropical SSTs between the high

and low NPO cases) would have reproduced the results of the control run. This was not the case, leading to the conclusion that the modulation effect is not explainable by tropical SSTs alone.

A low-pass filtered version of the NPO index and a high-pass filtered version of the ENSO index were used here, for consistency with GB. The intent was to enforce a time scale separation between the two phenomena. Two sensitivity tests were done to examine the influence of this filtering.

In the first sensitivity experiment, an unfiltered version of the NPO index was tried, and the control model's response evaluated as in Fig. 4. The results for the El Niño-high NPO, El Niño-low NPO, and La Niña-low NPO cases were little changed, being within about 0.5 mb of the results shown here. The La Niña-High NPO case showed a weaker anomaly in the Aleutian low region (2 mb vs. 5 mb), which made the La Niña case more like the El Niño case (and the observations) in terms of size of the NPO's effect. Overall, then, including the interannual variability in the NPO index results in a modestly larger modulation effect diagnosed from the control run. The composited SST fields using the unfiltered NPO index were virtually identical to those shown in Fig. 7. Given this, the modulation effect's forced response to these SST fields would likely have been similar to that found here, but another set of experiments to test this was not run.

In the second sensitivity experiment, an unfiltered version of the ENSO index was used. The main difference found in the control run was that warm tropical SSTs associated with El Niño extended farther to the west during low NPO conditions than during high NPO conditions (170°E versus 170°W, for the 1°C contour). By contrast, in the experiments

described here with the filtered ENSO index, there is little difference in tropical SSTs depending on the state of the NPO (Fig. 7). However, using these composite SST fields in another complete set of forced runs did not result in any different conclusions; i.e., there was again no significant forced SLP response in the Aleutian, southeastern U.S., or Atlantic regions.

It is worth explicitly mentioning the role of sampling in these results. Because of the large variability in midlatitude SLP, both the observations shown in Fig. 2 and (to a lesser extent, because of the greater sample size) the model results presented here are subject to sampling uncertainty. The formal way of addressing this is via the significance and K-S tests already performed. An informal but intuitively useful way of illustrating this issue is to examine random trials of the model data subsetted into the same sample sizes used in the observations. In particular, it was noted in section 3 that the model response was less similar to the observations during La Niña (compared to El Niño), because the model failed to reproduce the ridge of positive anomalies stretching from the central U.S. toward the Pacific Northwest. The observations for the La Niña case were formed from data from 5 winters (high NPO case) and 7 winters (low NPO case). Figure 13 shows the results of randomly sampling the model data during La Niña events (a pool of 27 and 34 winters for high and low NPO, respectively) into the same 5 and 7 samples as used in the observations, and then forming the difference between high and low NPO states. Six random trials were calculated. Interestingly, the ridge over the central U.S. and Pacific Northwest can clearly be seen in trial 4 (panel d), and hints of it can be seen in trials 1, 2, and 5. However, averaging over all the available samples nearly eliminates this feature. Given this and the

previous statistical tests, it is consistent with these results to conclude that the difference between the model results and observations is due to sampling errors associated with the observational record's length of 5 to 7 samples.

Furthermore, the statistical tests show that, for a given state of ENSO (either El Niño or La Niña), the *difference* in circulation anomalies between the high and low NPO cases are generally only significant in the Aleutian low region (Fig. 5), where the NPO itself has a significant effect. The limited exceptions to this are over the southeast U.S. during El Niño, and the far eastern Atlantic during La Niña. In other regions the circulation differences between high and low NPO states are consistent with a null hypothesis of sampling errors.

6. Conclusions

Observations show that ENSO's effects over North America in SLP and precipitation depend on the state of the NPO (Gershunov and Barnett 1998), which is here termed the "modulation" effect. Analysis of a 300-year control run of the parallel climate model showed that the model exhibits a similar modulation effect. However, this effect could not be reproduced by forcing the model with specified North Pacific SST anomalies. Therefore, it is concluded that the modulation effect arises because internal variability in the atmosphere both imprints in a characteristic way on North Pacific SSTs and alters ENSO's effects over North America. In such a case, neither accurate observations nor skillful predictions of future North Pacific SSTs will increase the forecast skill of ENSO's effects over North America.

Also tested was the possibility that the modulation effect arises from differences in tropical Pacific SSTs between different ENSO events, which might both force the NPO (or

NPO-like SST anomalies in the North Pacific) and alter the response over North America. It was found that part of the sea level pressure expression over the Aleutian region might be explained by this, but that tropical SSTs cannot by themselves explain all of the modulation effect.

As a final caveat, note that the model used here did not capture the full expression of the NPO/ENSO modulation effect seen in the observations. This study cannot rule out the possibility that the modulation effect is stronger in the real world because part of the response is directly forced by North Pacific SSTs, and the model's response is weaker than observed because it misses this part. Further studies with more accurate models, or perhaps cross-validated predictability studies of the observations, would be needed to address this question.

7. Acknowledgments

This work benefitted from talks with Tim Barnett, Niklas Schneider, and Alexander Gershunov of Scripps, which are gratefully acknowledged. Alexander Gershunov also provided the data that enabled the inclusion of Fig. 2. This work was supported by the Department of Energy's CCPP program (DE-FG03-91-ER61215). The computations were performed at NCAR's Climate Simulation Laboratory and the high performance computing facility at NERSC.

8. References

da Silva, A. M., C. C. Young, S. Levitus, 1995: Atlas of Surface Marine Data 1994, Volume 1: Algorithms and Procedures. NOAA Atlas NESDIS 6, U.S. Dept. Commerce, 299 pp.

Deser, C., M. L. Blackmon, 1995: On the Relationship between Tropical and North Pacific Sea Surface Temperature Variations. *J. Climate*, v. **8** p. 1677-1680.

Dukowicz, J. K., R. D. Smith, 1994: Implicit free-surface method for the Bryan-Cox-Semtner ocean model. *J. Geophys. Res.*, v. **99** p. 7991-8014.

Gershunov, A., T. P. Barnett, 1998: Interdecadal modulation of ENSO teleconnections. *Bull. Amer. Met. Soc.*, v. **79** p. 2715-25.

Hegerl, G. C., H. von Storch, K. Hasselmann, B. D. Santer, U. Cubasch, P. D. Jones, 1996: Detecting greenhouse-gas-induced climate change with an optimal fingerprint method. *J. Climate*, v. **9** p. 2281-306.

Horel, J. D., J. M. Wallace, 1981: Planetary-scale atmospheric phenomena associated with the Southern Oscillation. *Mon. Wea. Rev.*, v. **109** p. 813-829.

Hunke, E. C., J. K. Dukowicz, 1997: An elastic-viscous-plastic model for sea ice dynamics. *J. Phys. Oceanogr.*, v. **27** p. 1849-67.

Kiehl, J. T., J. J. Hack, G. B. Bonan, B. A. Boville, D. J. Williamson, P. J. Rasch, 1998: The National Center for Atmospheric Research Community Climate Model: CCM3. *J. Climate*, v. **11** p. 1131-1149.

Latif, M., T. P. Barnett, 1994: Causes of Decadal Climate Variability over the North Pacific and North America. *Science*, v. **266** p. 634-637.

Lau, N-C, 1985: Modeling the seasonal dependence of the atmospheric response to observed El Ninos in 1962-76. *Mon. Wea. Rev.*, v. **113** p. 1970-96.

Mantua, N. J., S. R. Hare, Y. Zhang, J. M. Wallace, R. C. Francis, 1997: A Pacific Interdecadal Climate Oscillation with Impacts on Salmon Production. *Bull. Amer. Met. Soc.*, v. **78** p. 1069-1079.

Mechoso, C. R., A. W. Robertson, N. Barth, M. K. Davey, P. Delecluse, others, 1995: The Seasonal Cycle over the Tropical Pacific in Coupled Ocean-Atmosphere General Circulation Models. *Mon. Wea. Rev.*, v. **123** p. 2825-2838.

Pierce, D. W., T. P. Barnett, N. Schneider, R. Saravanan, D. Dommenget, M. Latif, 2001: The role of ocean dynamics in producing decadal climate variability in the North Pacific. *Climate Dynamics*, v. **18** p. 51-70.

Press, W. H., B. P. Flannery, S. A. Teukolsky, W. T. Vetterling, 1992: Numerical recipes in Fortran, the art of scientific computing. Second edition. Cambridge university press, 963 pp.

Ropelewski, C. F., M. S. Halpert, 1986: North American precipitation and temperature patterns associated with the El Nino/Southern Oscillation (ENSO). *Mon. Wea. Rev.*, v. **114** p. 2352-62.

Schneider, N., A. J. Miller, D. W. Pierce, 2001: Anatomy of North Pacific decadal variability. *J. Climate, submitted.*

Smith, R. D., J. K. Dukowicz, R. C. Malone, 1992: Parallel ocean general circulation modeling. *Physica D*, v. **60** p. 38-61.

Wallace, J. M., D. S. Gutzler, 1981: Teleconnections in the geopotential height field

during the Northern Hemisphere winter. *Mon. Wea. Rev.*, v. **109** p. 784-812.

Washington, W. M., J. W. Weatherly, G. A. Meehl, A. J. Semtner, T. W. Bettge, A. P. Craig, W. G. Strand, J. Arblaster, V. B. Wayland, R. James, Y. Zhang, 2000: Parallel Climate Model (PCM) control and transient simulations. *Climate Dynamics*, v. **16** p. 755-74.

Zhang, J., W. D. Hibler, 1997: On an efficient numerical method for modeling sea ice dynamics. *J. Geophys. Res.*, v. **102** p. 8691-702.

Figure Captions

Figure 1. Top: ENSO sea surface temperature variability in the observations (left) and model (right), as represented by the leading EOF of annually averaged SST anomalies. Bottom: Same for the North Pacific Oscillation, as represented by wintertime (DJF) SST anomalies north of 20° N. Contours are in degrees C per standard deviation of the associated principal component. Contour interval is 0.25 C.

Figure 2. Observed mean sea level pressure anomalies (mb) composited on the state of ENSO and the North Pacific Oscillation. Replotted from Fig. 2 of Gershunov and Barnett (1998). Shading indicates significance at the 95% level. Contour interval is 1.0 mb.

Figure 3. Different between SLP anomalies in the high and low NPO cases, for El Niño conditions (left panel) and La Niña conditions (right panel).

Figure 4. Sea level pressure (mb) from the 300-yr control run, composited by the state of ENSO and the North Pacific Oscillation. Contour interval is 1.0 mb. Shading indicates values significantly different from zero at the 95% confidence level.

Figure 5. Difference between SLP anomalies in the high and low NPO states, for El Niño conditions (left panel) and La Niña conditions (right panel). Shading indicates a signal significantly different from zero at the 90% level.

Figure 6. Upper: Monthly averaged precipitation anomaly (10^{-9} m s^{-1}) for the 300-year control run, composited by the state of ENSO and the NPO (panels a through d). Lower: difference (high minus low NPO), for El Niño and La Niña conditions.

Figure 7. Sea surface temperature anomalies (°C) composited by the state of ENSO and the North Pacific Oscillation. Contour interval is 0.25°C.

Figure 8. Panels a) and b): SST anomaly (°C) from the 300-yr control run associated with the state of the NPO. Panels c) through f): the point-by-point sum of the SST anomaly associated with the model's NPO and ENSO. Contour interval is 0.25°C.

Figure 9. Upper: sea level pressure anomaly (mb) in the forced experiments composited by the state of ENSO and the North Pacific Oscillation. Lower: pressure difference (High - Low NPO) for the El Niño and La Niña cases. Contour interval is 1.0 mb. Shading indicates values significantly at the 95% confidence level.

Figure 10. Histograms of SLP anomaly during El Niño in the three regions of interest, when the NPO is high (solid lines) and low (dashed lines). The left hand column is from the control run, while the right hand column is from the forced (specified SST) runs. Also indicated is whether the two distributions are significantly different, as determined by a K-S test.

Figure 11. As in Fig. 8, but for La Niña conditions.

Figure 12. Upper: Monthly averaged precipitation anomaly (1.e-9 m/s) for the forced experiment, composited by the state of ENSO and the NPO (panels a through d). Lower: difference (high minus low NPO), for El Niño and La Niña conditions.

Figure 13. Differences in sea level pressure (mb) between high and low NPO cases, during La NiñaṪhe six trials were obtained by randomly sampling the model data using the same sample sizes as in the observations.

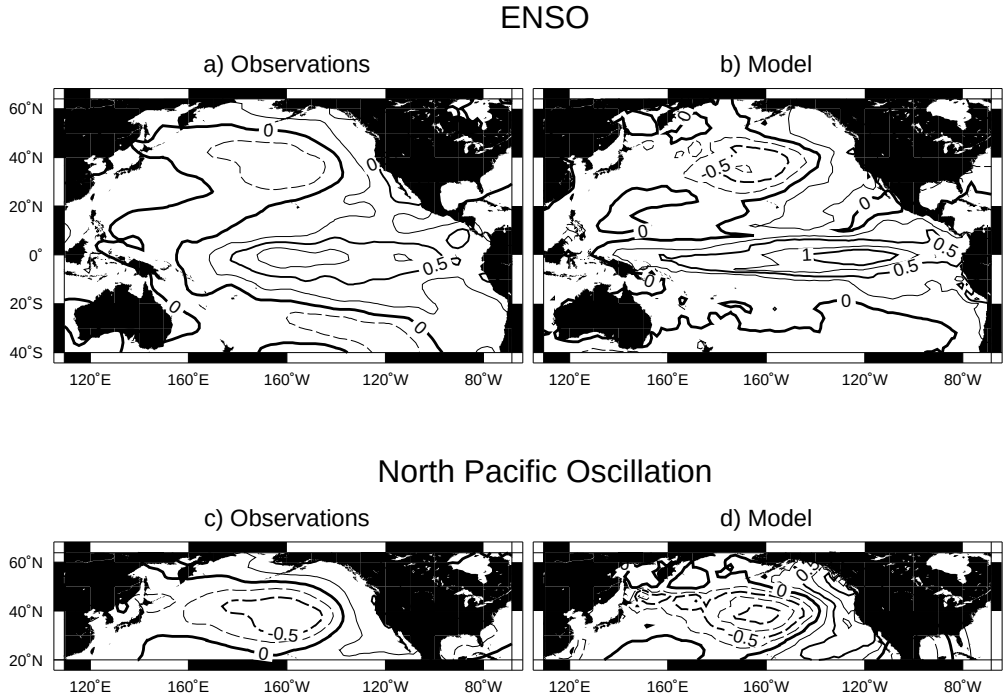
ENSO
a) Observations
b) Model
North Pacific Oscillation
c) Observations
d) Model
60˚N
40˚N
20˚N
0˚
20˚S
40˚S
120˚E
160˚E
160˚W
120˚W
80˚W

Figure 1:

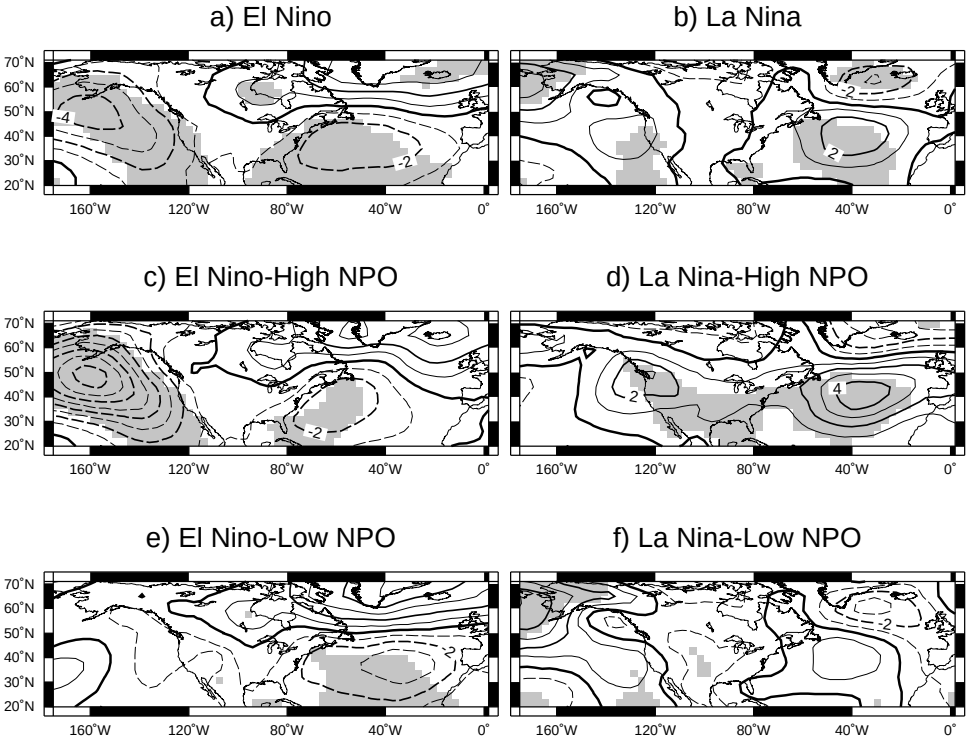
a) El Nino
b) La Nina
c) El Nino-High NPO
d) La Nina-High NPO
e) El Nino-Low NPO
f) La Nina-Low NPO
70°N
60°N
50°N
40°N
30°N
20°N
160°W
120°W
80°W
40°W
0°
-4
-2
2
4

Figure 2:

a) SLP Difference, El Nino

b) SLP Difference, La Nina

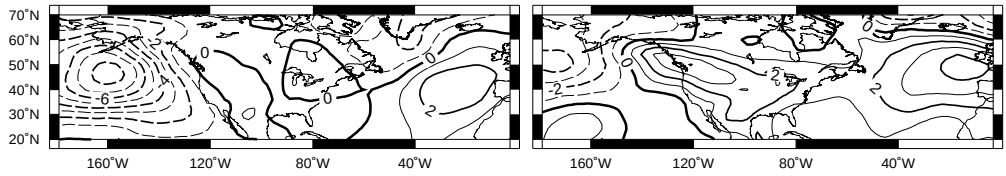

Figure 3:

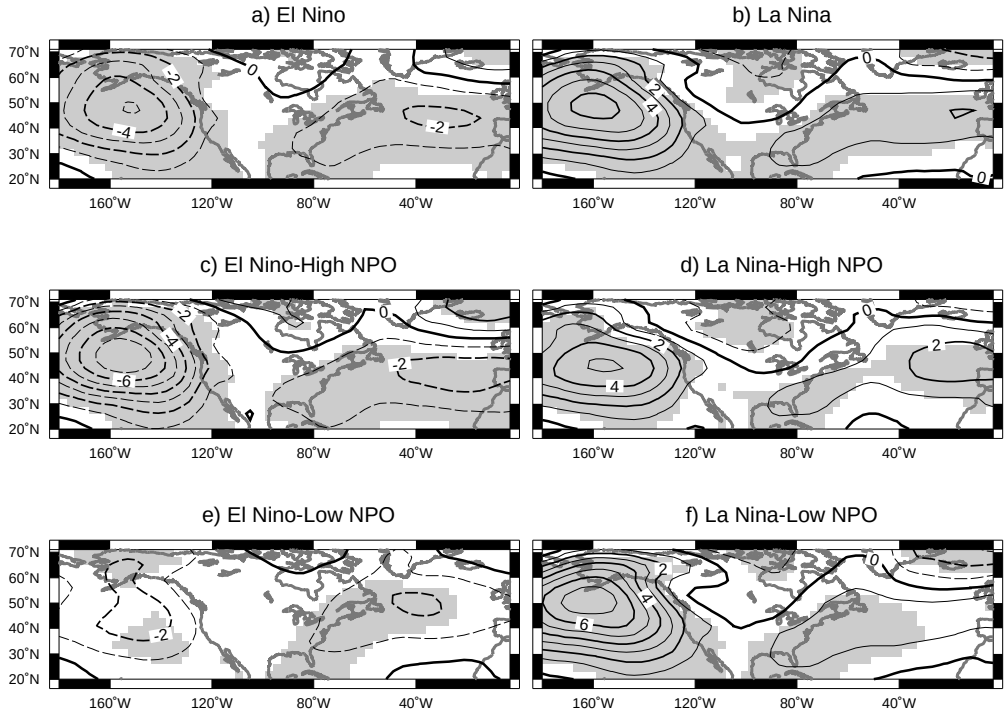
a) El Nino
b) La Nina
c) El Nino-High NPO
d) La Nina-High NPO
e) El Nino-Low NPO
f) La Nina-Low NPO
70°N
60°N
50°N
40°N
30°N
20°N
160°W
120°W
80°W
40°W

Figure 4:

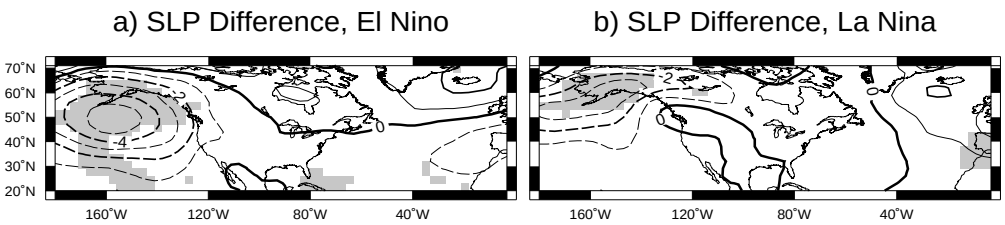
a) SLP Difference, El Nino
b) SLP Difference, La Nina
70˚N
60˚N
50˚N
40˚N
30˚N
20˚N
160˚W
120˚W
80˚W
40˚W
-4
-2
0
-2
160˚W
120˚W
80˚W
40˚W

Figure 5:

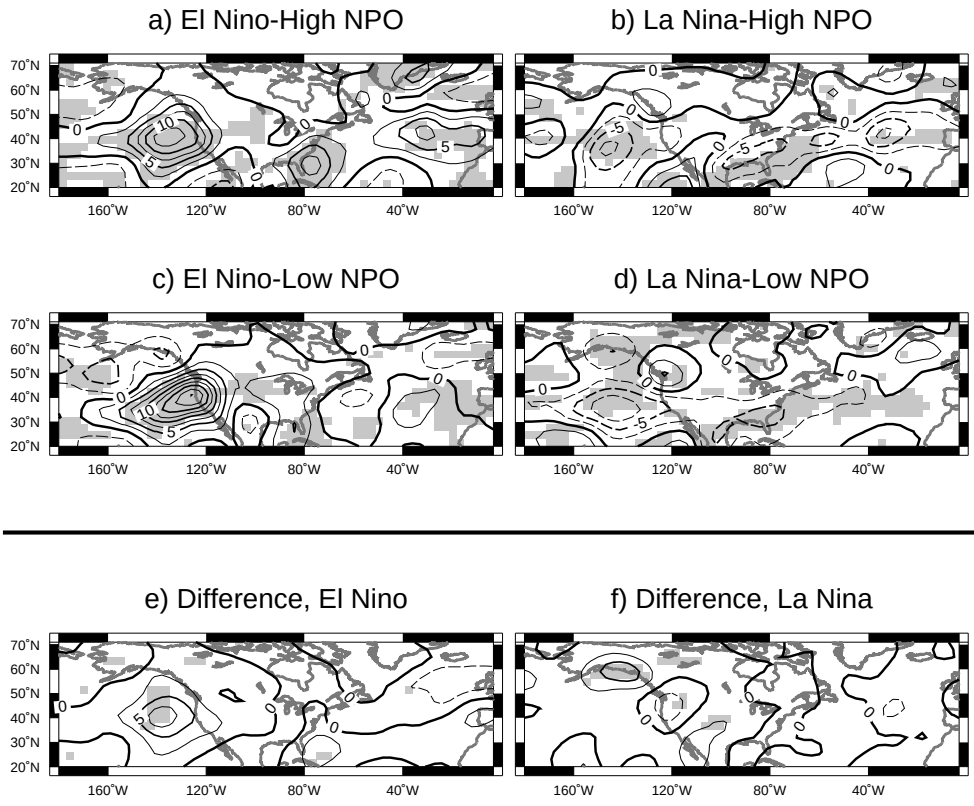
a) El Nino-High NPO
b) La Nina-High NPO
c) El Nino-Low NPO
d) La Nina-Low NPO
e) Difference, El Nino
f) Difference, La Nina
70°N
60°N
50°N
40°N
30°N
20°N
160°W
120°W
80°W
40°W

Figure 6:

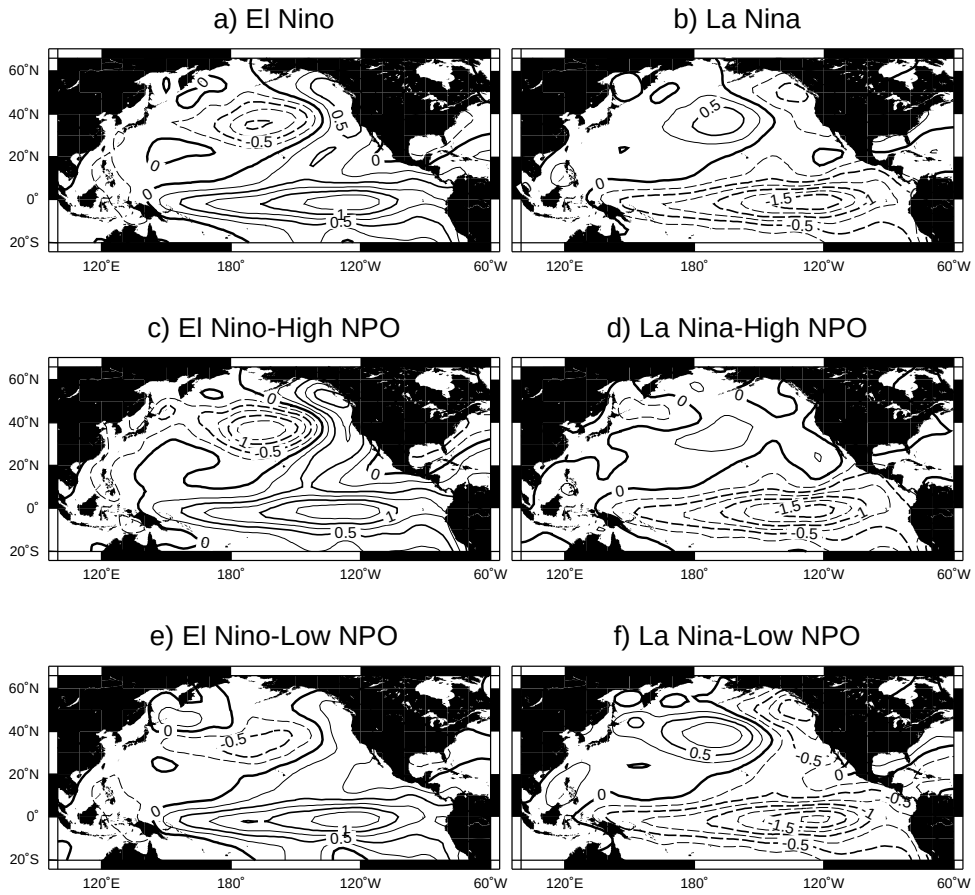
a) El Nino
b) La Nina
c) El Nino-High NPO
d) La Nina-High NPO
e) El Nino-Low NPO
f) La Nina-Low NPO
60°N
40°N
20°N
0°
20°S
120°E
180°
120°W
60°W

Figure 7:

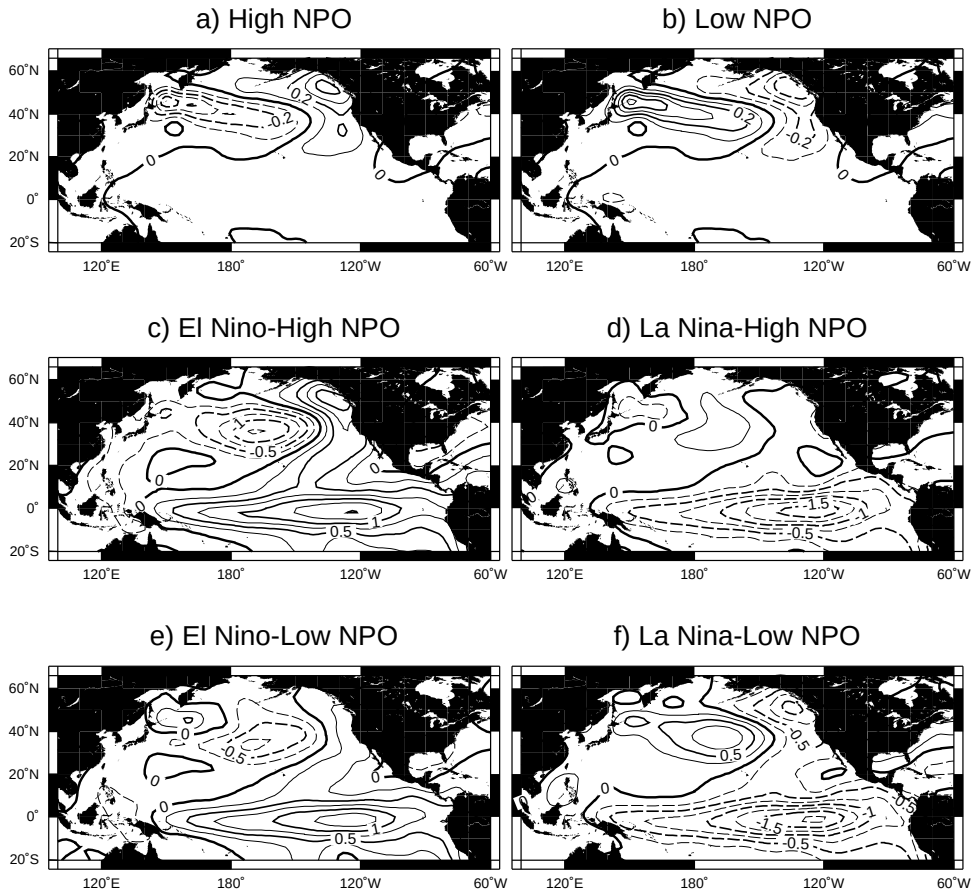
a) High NPO
b) Low NPO
c) El Nino-High NPO
d) La Nina-High NPO
e) El Nino-Low NPO
f) La Nina-Low NPO
60°N
40°N
20°N
0°
20°S
120°E
180°
120°W
60°W

Figure 8:

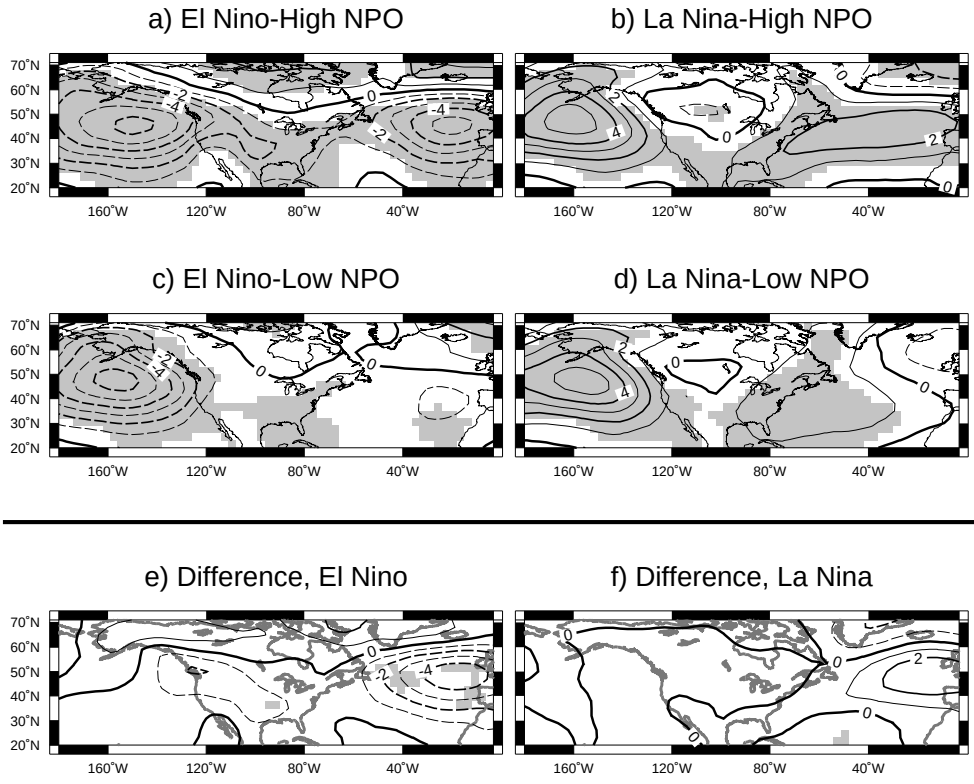
a) El Nino-High NPO
b) La Nina-High NPO
c) El Nino-Low NPO
d) La Nina-Low NPO
e) Difference, El Nino
f) Difference, La Nina
70°N
60°N
50°N
40°N
30°N
20°N
160°W
120°W
80°W
40°W

Figure 9:

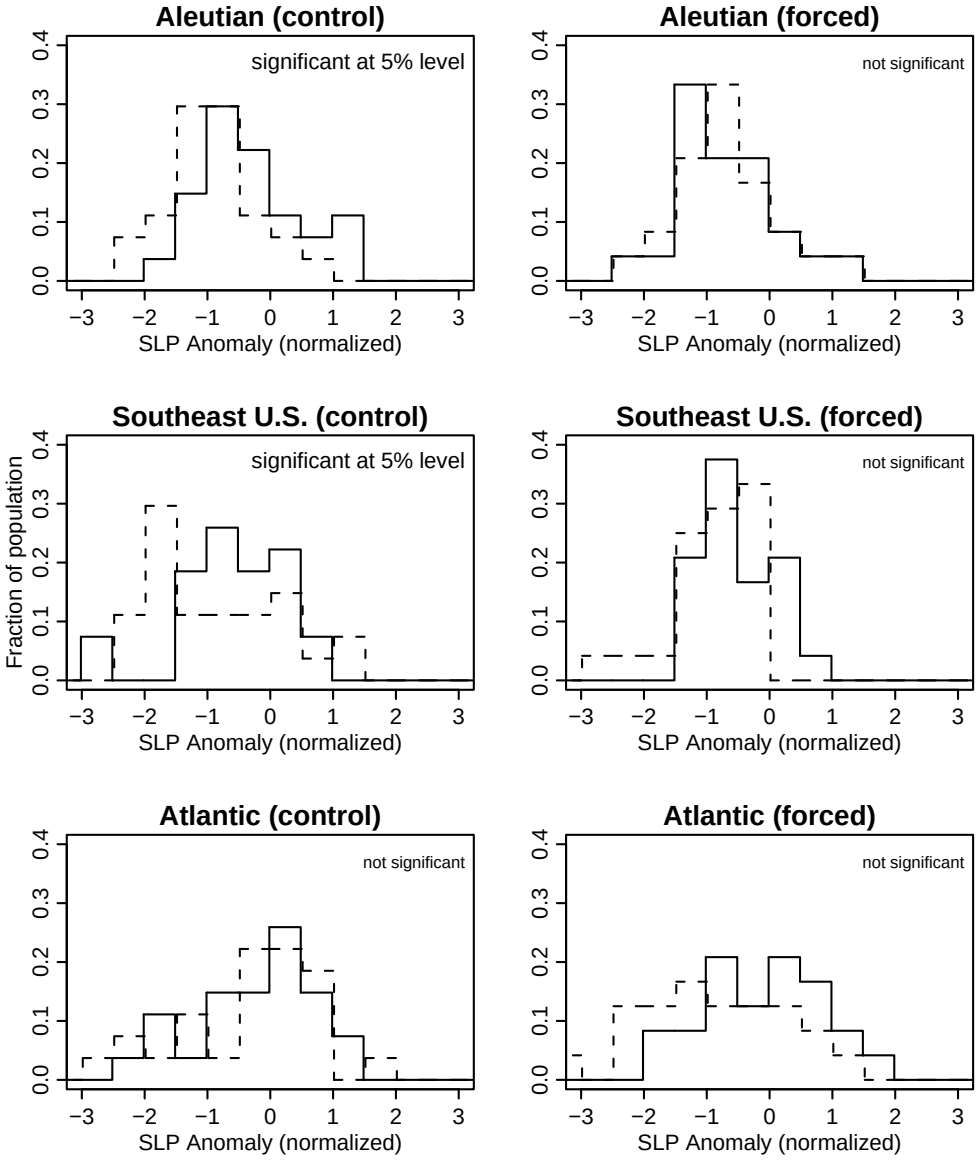
Aleutian (control)
significant at 5% level
Aleutian (forced)
not significant
Southeast U.S. (control)
significant at 5% level
Southeast U.S. (forced)
not significant
Atlantic (control)
not significant
Atlantic (forced)
not significant
Fraction of population
SLP Anomaly (normalized)
0.0
0.1
0.2
0.3
0.4
−3
−2
−1
0
1
2
3

Figure 10:

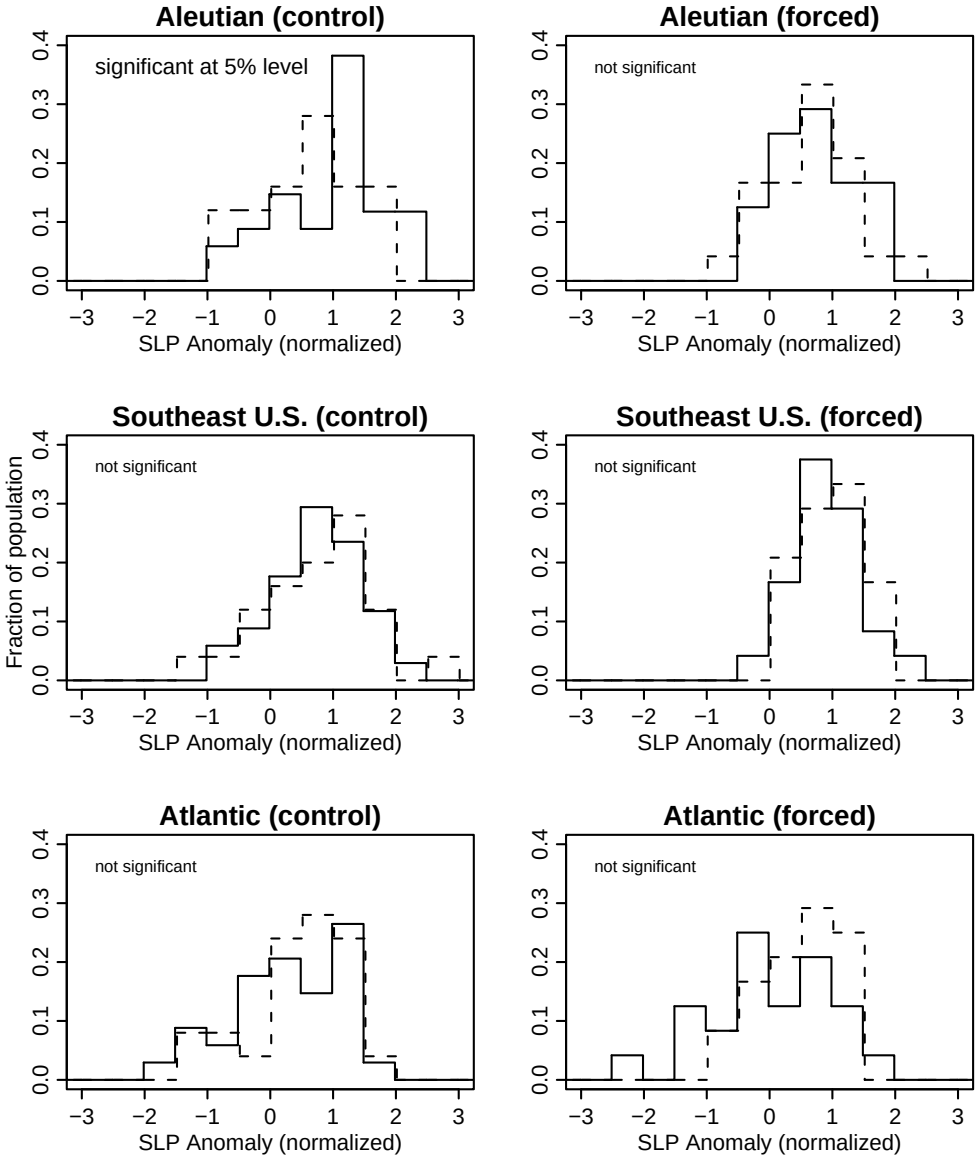
Aleutian (control)
significant at 5% level
Aleutian (forced)
not significant
Southeast U.S. (control)
not significant
Southeast U.S. (forced)
not significant
Atlantic (control)
not significant
Atlantic (forced)
not significant
Fraction of population
SLP Anomaly (normalized)

Figure 11:

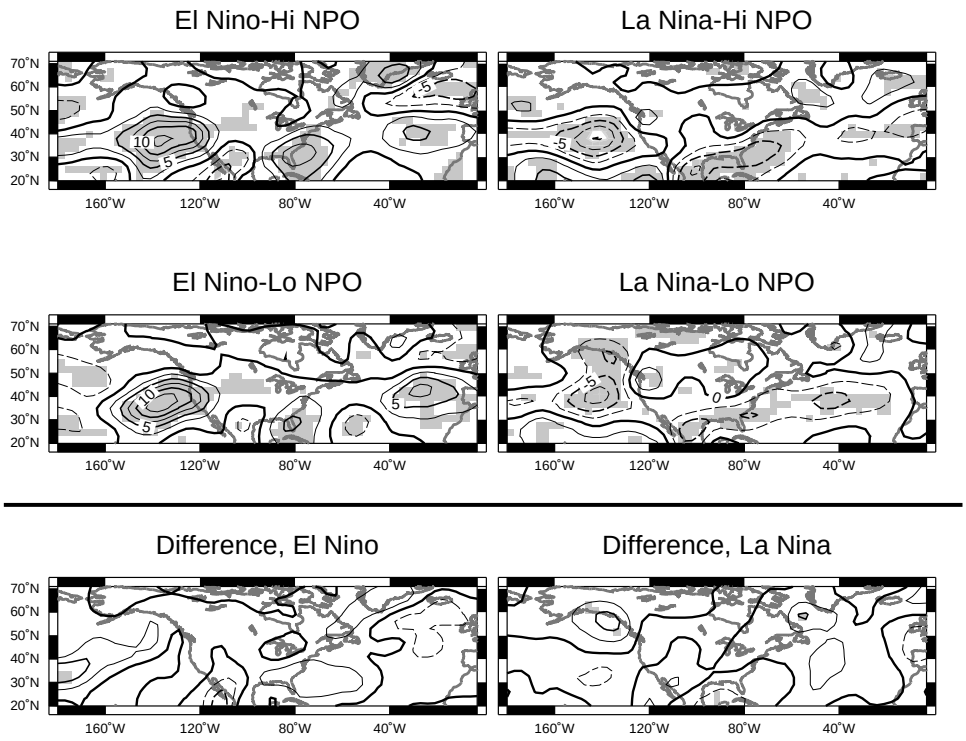
El Nino-Hi NPO
La Nina-Hi NPO
El Nino-Lo NPO
La Nina-Lo NPO
Difference, El Nino
Difference, La Nina
70°N
60°N
50°N
40°N
30°N
20°N
160°W
120°W
80°W
40°W

Figure 12:

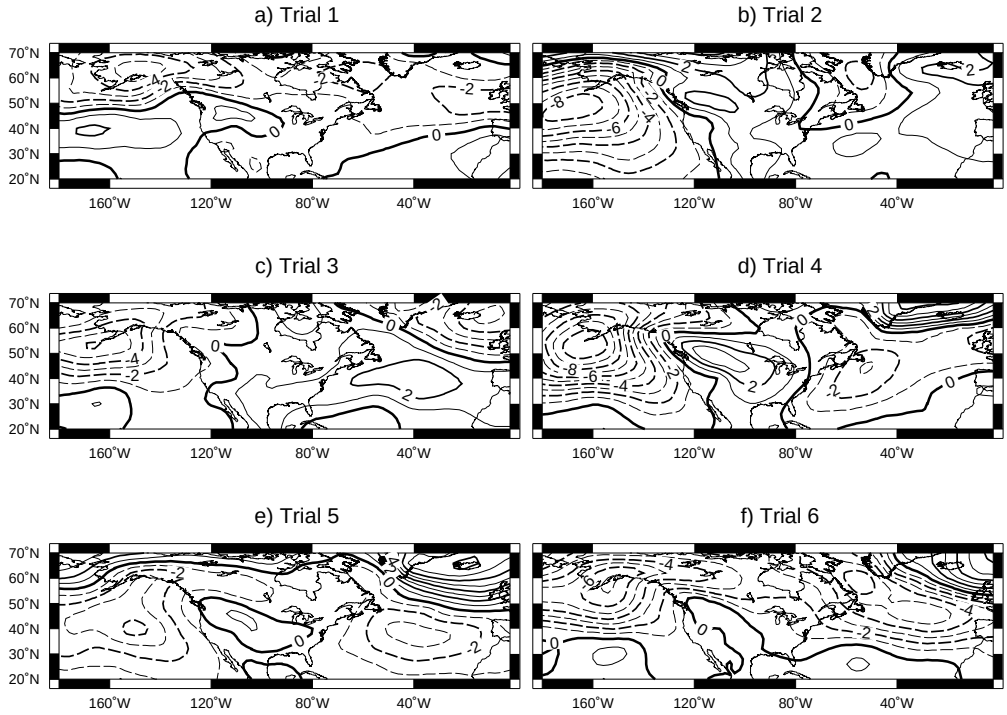
a) Trial 1
b) Trial 2
c) Trial 3
d) Trial 4
e) Trial 5
f) Trial 6
70°N
60°N
50°N
40°N
30°N
20°N
160°W
120°W
80°W
40°W

Figure 13: